

ABSTRACT

Mehta, Kurang. Numerical Methods to Implement Time Reversal of Waves Propagating in Complex Random Media. (Under the direction of Dr. J P Fouque (MATH Department) and Dr. Gianluca Lazzi (ECE Department)).

A time reversal mirror is a device capable of receiving a signal in time, keeping it in memory, and sending it back into the same medium in the reversed direction of time. The main effect is the fascinating refocusing of the scattered signal, which is formed by sending the pulse into a complex medium, after time reversal through the same medium. The refocused signal is a pulse with shape similar to the initial pulse along with some low amplitude noise. This surprising effect has a great potential for application in domains such as medical imaging, underwater acoustics and wireless communication.

Time reversal is studied in reflection and transmission. In both cases, we demonstrate the self-averaging properties of the time reversed refocused pulse. An accurate numerical method for simulating waves propagating in complex one-dimensional media is employed. Numerical simulations are used to reproduce the time-reversal self-averaging effect which takes place in randomly layered media. The effect of refocusing is enhanced in a regime where the inhomogeneities are smaller than the pulse, which propagates over long distances compared to its width.

Time Reversal can be implemented using several numerical methods including Transfer Matrix, Finite Difference Time Domain (FDTD) & Boundary Integral Methods. This

thesis includes a comprehensive comparison of the methods in terms of speed and accuracy.

The most efficient method for implementing time reversal is then used to obtain numerical evidence for potential use of a sliding window time-reversal technique for detecting a buried cavity/object inside the medium. The numerical methods are well adapted for generalization to the multi-dimensional case.

Numerical Methods to Implement Time Reversal of Waves Propagating in Complex

Random Media

by

Kurang Mehta

A thesis submitted to the Graduate Faculty of
North Carolina State University
in the partial fulfillment of the
requirements for the degree of
Masters of Science

Electrical Engineering

Raleigh, NC

May 15, 2003

APPROVED BY:

Dr. Gianluca Lazzi

Chair of Advisory Committee

Dr. Jean-Pierre Fouque

Co-chair of Advisory Committee

Dr. Mansoor Haider

Dr. Michael Steer

Biography

Kurang Mehta was born on April 30, 1979 in Baroda, India. He completed his schooling at Shreyas Vidyalaya in May 1997. He graduated from Maharaja Sayajirao University of Baroda, India in May 2001 with a bachelor's degree in Electronics and Communications Engineering. He received his M.S in Electrical Engineering from North Carolina State University, in August 2003. His interests are in wave propagation and scattering of waves in complex media.

Acknowledgements

I would like to thank my advisor Dr. Gianluca Lazzi and my co-advisor Dr. Jean-Pierre Fouque along with Dr. Mansoor Haider without whose guidance and help this thesis would have but remained a dream. I thank them for their patience, support, advice and encouragement.

Contents

List of Figures.....	vii
-----------------------------	------------

List of Tables.....	ix
----------------------------	-----------

1. INTRODUCTION	1
1.1 Motivation.....	1
1.2 Overview of Time Reversal.....	3
1.3 Model.....	4
1.4 Scales.....	4
1.5 Methods used to Implement Time Reversal.....	5
1.6 Applications of Time Reversal.....	7
 2. TRANSFER MATRIX METHOD	 10
2.1 Method.....	10
2.2 Implementation.....	12
2.3 Train of Pulses.....	15

3. FINITE DIFFERENCE TIME DOMAIN METHOD	19
3.1 Introduction.....	19
3.2 Formulation of Equations.....	20
3.3 Boundary Conditions and Higher Order Accurate Schemes.....	22
3.4 Algorithm.....	23
3.5 Results.....	25
3.6 Different Realizations using Various Random Media.....	28
3.7 Numerical Convergence and Time Considerations.....	29
 4. BOUNDARY INTEGRAL METHOD	 31
4.1 Introduction.....	31
4.2 Assembly of the System of Equations.....	32
4.3 Pulse Refocusing and Random Realizations.....	35
4.4 Effect of Increasing the Number of Layers.....	36
4.5 Verification of the Theoretical Formula.....	39

5. DETECTION OF A BURIED CAVITY VIA TIME-REVERSAL	43
5.1 Hypothesis.....	43
5.2 Experiments.....	43
5.3 Statistical Analysis of the Time Reversed pulse amplitude.....	47
 6. CONCLUSIONS AND FUTURE WORK	 51
 7. REFERENCES	 53

List of Figures

2.1 Initial Gaussian pulse.....	13
2.2 Velocity distribution of the random medium.....	13
2.3 Response of the random medium to unit impulse input.....	14
2.4 Reflected signal when a Gaussian pulse interacts with the random medium.....	14
2.5 Refocused pulse.....	15
2.6 Train of Gaussian pulses $\{1,0,1,0,0,1\}$	16
2.7 Reflected signal when the Gaussian pulses interacts with the medium.....	17
2.8 Refocused train of pulses.....	18
3.1 Distribution of the velocity of propagation of the random medium.....	25
3.2 Initial Gaussian pulse.....	26
3.3 Reflected and transmitted signal when the pulse interacts with medium.....	26
3.4 Refocused pulse.....	27
3.5 Magnified view of the refocused pulse.....	28
3.6 10 Random realizations of the refocused pulse.....	28
4.1 Refocused pulse.....	35
4.2 10 Random realizations of the refocused pulse.....	36
4.3 10 Random realizations of the refocused pulse (N=5).....	37
4.4 10 Random realizations of the refocused pulse (N=10).....	37
4.5 10 Random realizations of the refocused pulse (N=20).....	37

4.6 10 Random realizations of the refocused pulse ($N=50$).....	37
4.7 10 Random realizations of the refocused pulse ($N=100$).....	38
4.8 10 Random realizations of the refocused pulse ($N=300$).....	38
4.9 Verification of theoretical formula for different number of layers.....	41
5.1 Comparison of pulse amplitude with and without cavity.....	44
5.2 Comparison of pulse amplitudes with and without cavity for 50 realizations.....	45
5.3 % difference of the amplitudes with and without cavity ($L=50$) for 50 realizations...	46
5.4 % difference of the amplitudes ($L=20, 10, 4$) for 50 realizations.....	47

List of Tables

1 Study of effect of increasing the number of layers for 25 different realizations.....	38
2 Comparative study of the three methods in terms of speed and accuracy.....	42
3 Statistics of time-reversed pulse amplitude for different size of object/ cavity for number of layers $N=100$	48
4 Statistics of time-reversed pulse amplitude to analyze the extent to which the detection measure can indicate the depth of buried cavity for $N=100$	49

1. INTRODUCTION

1.1 MOTIVATION

Ground penetration radar (GPR) has been an important tool for buried – target detection and identification over the last several decades [21]. In most GPR systems which use antennas, the buried target is generally in the near zone of the often complicated antenna pattern. It is often used to acquire information and solve problems without any necessity to process or model the data (such as locating the horizontal location of a buried pipe). However, when logistical constraints, geometry problems, excess noise, equipment artifacts, or properties of the ground cause distortions of the radar data, then data processing may be required to correct or enhance the radar images. Processing may also be required to extract quantitative information such as descriptions of statistical heterogeneity or to extract information from multiple geometries of data acquisition (as in tomography). When quantitative information is required about size, shape and depth of buried objects or structures, and when material properties are required, then modeling of ground penetrating radar may be necessary. Modeling is also useful in predicting GPR performance before going to field sites.

GPR can be used to detect buried targets which are in the near zone. Another tool recently developed for buried mine detection is the synthetic aperture radar (SAR). The SAR system has a significant standoff distance and since the targets are in the far zone of

the source, relatively simple antenna designs can be used for detection. SAR instruments use pulses of microwaves as an active source of illumination [28], [27]. The properties of microwaves are also quite distinct from electromagnetic radiation in the optical and IR part of the spectrum. SAR systems can see through clouds, for instance, and as active systems they can image both during day and night. In addition, the singular nature in which microwaves interact with surface features means that information obtained in SAR images is quite different from the reflectivity measured in optical and IR imagers. While a SAR system may have difficulty detecting all individual mines, it can be an effective tool for mine-field detection. Also one principal limitation of the SAR system is the ability of the electromagnetic waves to penetrate lossy soil. Thus, there has been much interest in this field in developing new tools that can help overcome some of the above limitations. Time Reversal shows a promise to be used as a detecting technique in environments where detection becomes difficult for other devices.

This work has been undertaken to address recent advances in the field of detection and results in the development of an application of “Time Reversal Mirrors” as a buried target detector.

1.2 OVERVIEW OF TIME REVERSAL

A time reversal mirror is a device that is capable of receiving an acoustic signal in time, keeping it in memory, and sending it back into the same medium in the reversed direction of time. The main effect is the refocusing of the scattered signal after time reversal in random media. This scattered signal is formed by sending a pulse into a disordered medium. The refocused signal is a pure pulse with a shape similar to the initial pulse.

A fundamental property of waves is that when two of them pass through the same location, they reinforce each other if their peaks and troughs correspond and they tend to cancel each other out if the peaks of one combine with the troughs of the other. For implementing time reversal, a wave transmitted through the random medium is recorded on a small time-reversed mirror and sent back into the medium, time reversed. Our analysis enables us to contrast the refocusing properties of a homogenous medium and a random medium. The fluctuations in the random medium actually enhance the spatial refocusing around the initial source position. A regime is considered in which the correlation length of the medium is much smaller than the pulse width, which itself is much smaller than the distance of propagation.

Such mirrors have a wide range of applications including destruction of tumors and kidney stones, detection of defects in metals, long distance secure communication and mine detection in the ocean. As of today the only waves for which Time Reversal devices

exist are ultrasonic waves. For other types of waves (e.g. wireless communications) we, at present, rely on computational Time Reversal methods.

1.3 MODEL

Our model domain is characterized by the velocity of propagation of the wave. The velocity of propagation is defined as:

$$1/c^2(x) = 1/c_0^2 * (1 + \mu(x/\varepsilon)) \quad (1.1)$$

where c_0 is the velocity of wave propagation in free space, $\mu(x/\varepsilon)$ is a function of the position x and $\varepsilon = 1/N$ with N as the number of layers.

At the interface, we have matched the constant medium on the left with the averaged medium on the right in the sense that

$$1/c_0^2 = \langle 1/c^2(x) \rangle \quad (1.2)$$

This is the interface condition imposed to make the boundary value problem simpler and avoid jumps while solving the wave equation at the interface.

1.4 SCALES

The refocusing is obtained by using asymptotics in the regime where there are three well separated scales:

$$l \ll \lambda \ll L \quad (1.3)$$

where l is the correlation length of the medium, λ is the wavelength of the pulse and L is the distance of propagation.

Scales are very important for the time reversal effect. Any violation of the above scales leads to homogenization of the medium which inhibits the time reversal effect.

Time reversal and the randomness in the medium help in beating the diffraction limit. This effect is called super-resolution, and has various applications in imaging and wireless communication.

1.5 METHODS USED TO IMPLEMENT TIME REVERSAL

The three methods that are used here to implement time-reversal in one-dimension are the Transfer Matrix Method, Finite Difference Time Domain Method and Boundary Integral Method.

The Transfer Matrix Method, a natural method to solve the wave equation for problems involving interfaces, has certain drawbacks:

- This method needs the reflected pulse along with the whole array of random media to be stored and used at each step of propagation. Convolution operation at each time step uses a lot of memory and slows the execution.
- As this method is an iterative method which tracks the multiple scattering, it is not possible to take into account all the scattered pulses. This reduces accuracy of the results and leads to increased noise accompanying the refocused signal.
- The Transfer Matrix Method is easy to implement for solving problems in the 1-D case but the computational complexity increases significantly when we move to higher dimensional layered problems. This is because it is required to track the multiple scattering of waves at each layer.

The Finite Difference Time Domain Method partitions the domain into a grid to discretize the wave equation as written in the differential form. This method has the following advantages:

- One of the possible finite difference schemes is the explicit (2,4) scheme. This scheme discretizes the wave equation to second order accuracy in time and fourth order accuracy in space. The explicit nature of the scheme makes it easy to implement.
- This method is versatile and can be extended to higher dimensions as well as non-linear problems since it is based on discretizing the governing partial differential equation.

There are some limitations of this method. As this method requires full spatial and time discretization, the computational complexity is higher compared to the other two methods. Parametric analysis for any problem will require the execution for multiple realizations. This makes the parametric analysis for any time reversal problem time consuming.

The Boundary Integral Method is based on Green's functions and, in one spatial dimension, is much faster than the Finite Difference Time Domain Method. In the Boundary Integral Method, the interface conditions are automatically satisfied. However, there are certain drawbacks of this method which are:

- This method is restricted to solving problems which are linear in nature due to the use of Green's functions.

- One should be beware of ill-conditioning while using this method, particularly for large scale problems. Also, for large scale problems, evaluation of the Green's function is tedious.

1.6 APPLICATIONS OF TIME REVERSAL

The refocusing of the time reversed pulse is independent of the realization of the random medium when the three scales: the extent of the random medium, the width of the pulse and the width of the each layer are well separated. This pulse refocusing property can be employed in several applications.

- **Secure communication**

Time reversal can be used for secure communication since after passing through the random complex medium the pulse gives rise to a transmitted signal and a reflected signal which does not carry any detectable information about the medium or the data transmitted. This reflected signal, when time-reversed and passed through the same medium, will give rise to a refocused pulse similar to the original pulse in shape and size. While communicating we can put our random media at the two ends of our communication system and hence transmit our information (which are pulses originally) in the form of apparent noise, hence making the transmission more secure.

- **Medical applications (Kidney Stone Destruction and Tumor Detection)**

Among the medical applications of pulse echo Time Reversal Mirrors, the closest to fruition is the destruction of stones in kidney and tumors. Conventional ultrasonic or X-ray imaging can accurately locate such objects, but it is difficult to focus ultrasonic waves through the surrounding tissues to destroy the stones, as these tissues may make the problem non-linear in nature. Also, the movement of stones during breathing is hard to track [14]. Only an estimated 30 percent of the shots reach the stone and it takes several thousand shots to destroy one. Ultrasonic Time Reversal techniques can solve the problem. Another promising application is ultrasonic medical hyperthermia (unwanted fever that can result for instance during anesthesia and lead to patient death), in which high-intensity ultrasound heats up tissues. Temperature above 60 degrees Celsius (140 degree Fahrenheit) can destroy tissues within seconds [4]. Devices using conventional techniques to focus ultrasound waves can be useful for static tissues such as cancerous prostate glands. Time Reversal Mirrors can be used to overcome this limitation and hence make the conventional techniques useful even for non-static tissues.

- **Underwater object detection**

The principle for underwater object detection remains the same as in detection of tumors [14]. A pulse is sent underwater which interacts with the medium and gives rise to a reflected pulse. We then time reverse it and send it back into the same medium. The pulse which comes out of the medium can then be studied and hence used to detect underwater objects.

- **Detection of defects in the medium**

Another important application of Time Reversal Mirrors is flaw detection in solids by non-destructive evaluation. Small defects are hard to find in an object with a complicated geometry or one made of heterogeneous or anisotropic material [14]. Usually the sample and the ultrasonic transducers are immersed in water, but refraction can alter the beams at the water-solid interface, making it even harder to detect small defects. Furthermore, the ultrasound can produce a variety of wave polarizations and types in the solid. Time Reversal Mirrors can automatically compensate for these problems.

- **Imaging Underground**

The principle used for underwater object detection can also be used to image underground objects, the only difference being that the medium will be different. This can be used for non-destructive imaging of objects underground.

2. TRANSFER MATRIX METHOD

This is a natural method used to solve the wave equation in problems involving interface and boundary conditions since it directly tracks the multiple scattering of waves as they interact with the random medium. The Transfer Matrix Method is an iterative method involving discretization of the model domain into different layers having different velocities of propagation.

2.1 METHOD

The random medium is first divided into various sub-layers having different velocities. We denote each velocity by $\{c_i\}$ where 'i' indicates the index of layer in the random medium. The velocities are selected randomly using the formula:

$$c_i = c_0 / \sqrt{1 + X_i} \quad (2.1)$$

where X_i is an independent identically distributed (IID) random variable uniformly distributed over $(-\sigma, \sigma)$ where σ can take any value between 0 and 1. The velocity outside the medium is taken as $c=1$.

The Transfer Matrix method is based on the fact that when a pulse with amplitude 'a' is incident on an interface having velocity of propagation c_2 on its right and c_1 on its left, the reflected pulse has amplitude:

$$a_r(c_1, c_2) = a(c_2 - c_1) / (c_2 + c_1) \quad (2.2)$$

and the transmitted pulse has amplitude:

$$a_t(c_1, c_2) = a(2c_1) / (c_2 + c_1) \quad (2.3)$$

In this iterative method, we find the amplitudes of the reflected signal at different times 't' at the previous layer $R((N-i-1)\varepsilon, t)$ using the value of the reflected signal at the current layer $R((N-i)\varepsilon, t)$ where ε is the width of each of the layers ($= 1/N$), N is the number of layers, 'i' is the current layer and 't' is the current time.

The amplitude in the last layer is given by:

$$R(N\varepsilon, t) = a_r(C_N, 1) * \delta_0(t) \quad (2.4)$$

where $*$ indicates convolution and $\delta_0(t)$ is an impulse function centered at zero.

This implies that the amplitude at time $t=0$ is $a_r(C_N, 1)$.

We can generalize a formula to find the reflected signal for any specific layer 'i' since the amplitude of the reflected signal at any given layer depends on the amplitude of the layer to its immediate left. We can use this property to construct an iterative formula.

If we know the amplitude in layer (N-i) then we can find the amplitude in the layer (N-i-1) using the following iterative formula:

$$R((N-i-1)\varepsilon, t) = a_r(C_{N-i-1}, C_{N-i}) * \delta_0(t) + \sum_{k=1}^N [a_t(C_{N-i-1}, C_{N-i}) * a_t(C_{N-i}, C_{N-i-1}) * R((N-i)\varepsilon) * \delta_{2k\varepsilon/CN}(t) * a_r^{(k-1)}(C_{N-i}, C_{N-i-1})] \quad (2.5)$$

This equation can be used to find the amplitudes at each layer starting from the rightmost layer. Instead of taking all N terms, we can truncate the number of terms to M where M is any integer less than N. We will then have the response of the medium to an impulse of given amplitude.

2.2 IMPLEMENTATION

For implementing time reversal in 1-D using the Transfer Matrix Method, we can start with any pulse. Here the pulse used is a Gaussian pulse, having zero mean and variance ($= \varepsilon$), defined by the equation:

$$f(t/\sqrt{\varepsilon}) = - (t/\sqrt{\varepsilon}) * \exp(-t^2/2 * \varepsilon) \quad (2.6)$$

which can be viewed in Fig.2.1.

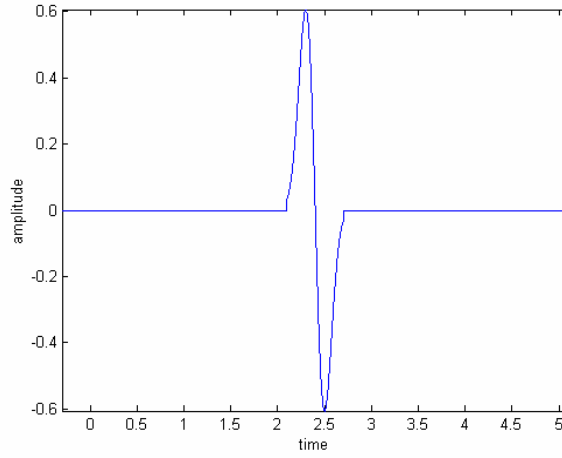


Figure 2.1 Initial Gaussian pulse

The random medium is generated using Equation (2.1). Here the value of σ is chosen to be 0.5. We see that this leads to $X_i \in [-0.5 \ 0.5]$ which results in the velocity of propagation varying between 0.866 and 1.414. The plot of velocities of propagation in the random media can be viewed in Fig.2.2.

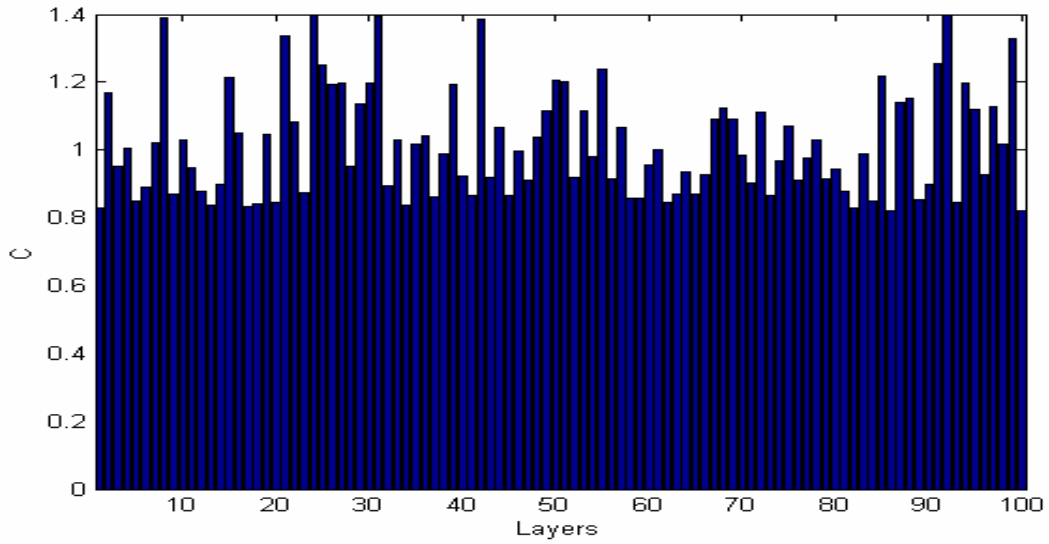


Figure 2.2 Velocity distribution of the random medium

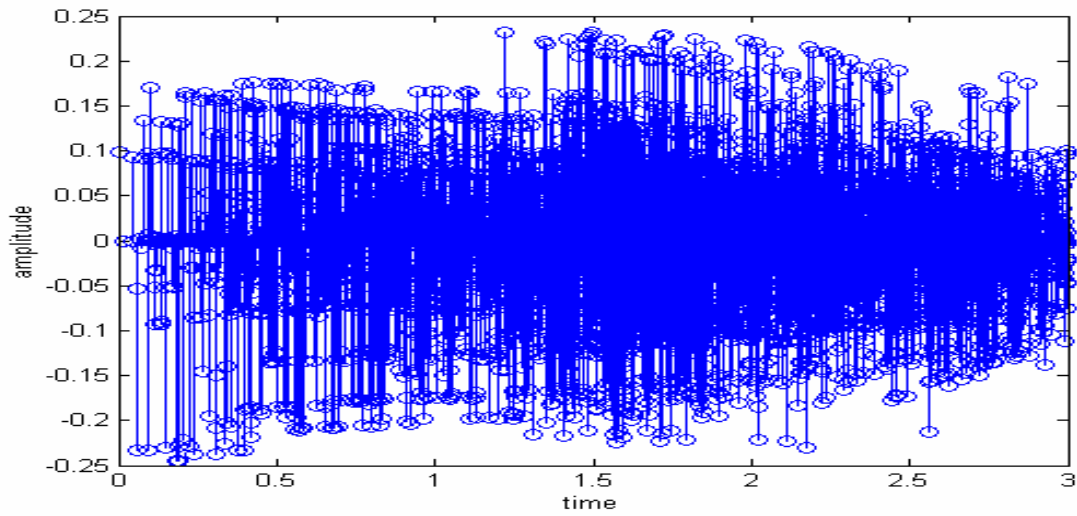


Figure 2.3 Response of the random medium to unit impulse input

Fig 2.3 shows the response of a unit impulse when passed through the medium shown in Fig 2.2. When the gaussian pulse shown in Fig.2.1 passes through the random medium, we get the response of the random medium. This is a very complicated signal which is a convolution of the pulse with the random medium and is shown in Fig.2.4.

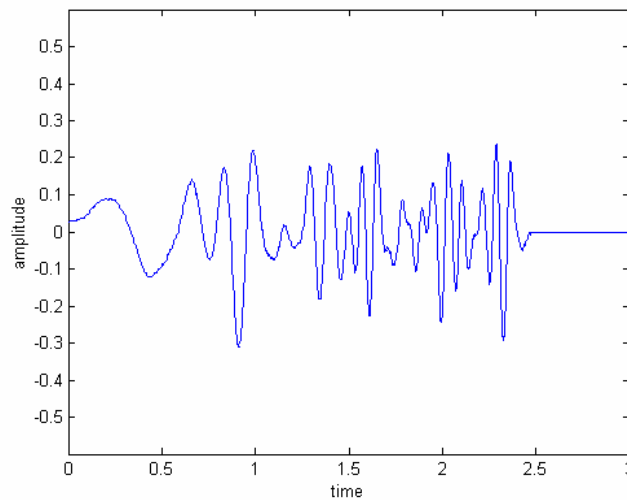


Figure 2.4 Reflected signal when a Gaussian pulse interacts with the random medium

This signal (or a window of it) is then reversed in time, that is, the part of the signal which came out of the medium first will re-enter the medium last, and vice versa. The time reversed signal is then re-introduced into the same medium. The pulse that comes out of the medium is again a convolution of the windowed complicated signal and the random medium and will be similar in shape to the original pulse with a low amplitude coda that can be seen in Fig.2.5.

2.3 TRAIN OF PULSES

We can also implement this method for a train of pulses. Here, instead of a single pulse, we use a train of pulses, as shown in Fig.2.6. Compared to one pulse, a train of pulses can carry considerably more information, and hence we can use the technique efficiently for secure communication. Here the sequence is $\{1,0,1,0,0,1\}$.

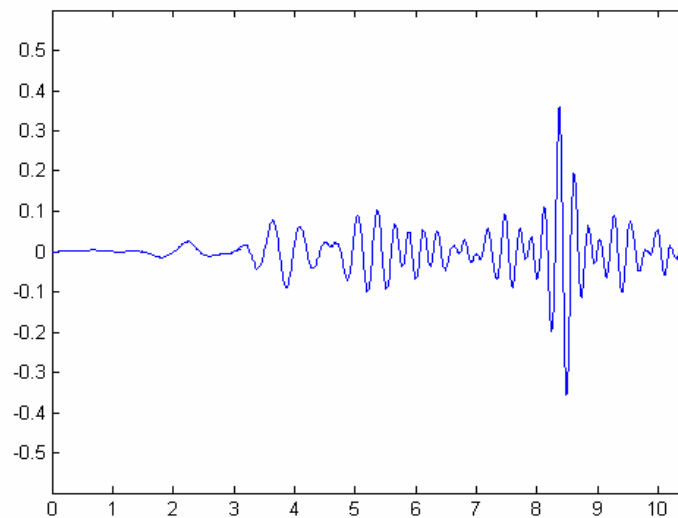


Figure 2.5 Refocused pulse

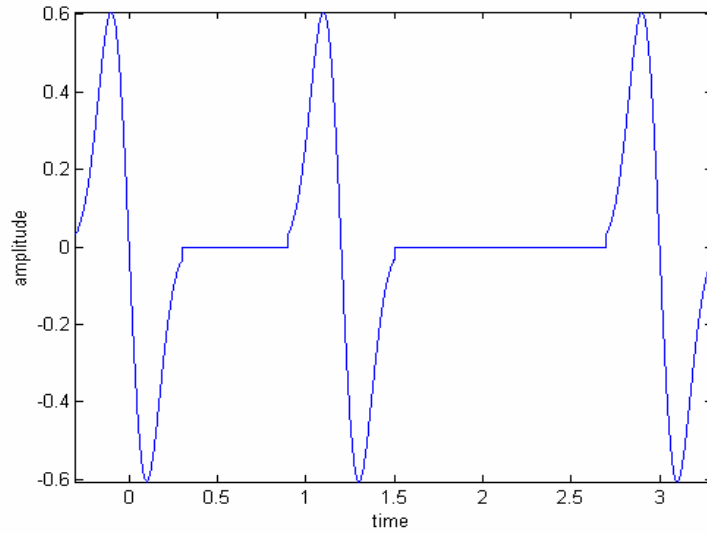


Figure 2.6 Train of Gaussian pulses $\{1,0,1,0,0,1\}$

The pulse which goes first into the medium will come out last from the medium after time reversal. The scales should always be kept in mind ($\varepsilon^2 \ll \varepsilon \ll 1$ where ε is the standard deviation of the original pulse and ε^2 is the correlation length of the medium).

This train of pulses interacts with the random medium as shown in the Fig.2.2 and gives out the reflected signal which can be viewed in Fig 2.7.

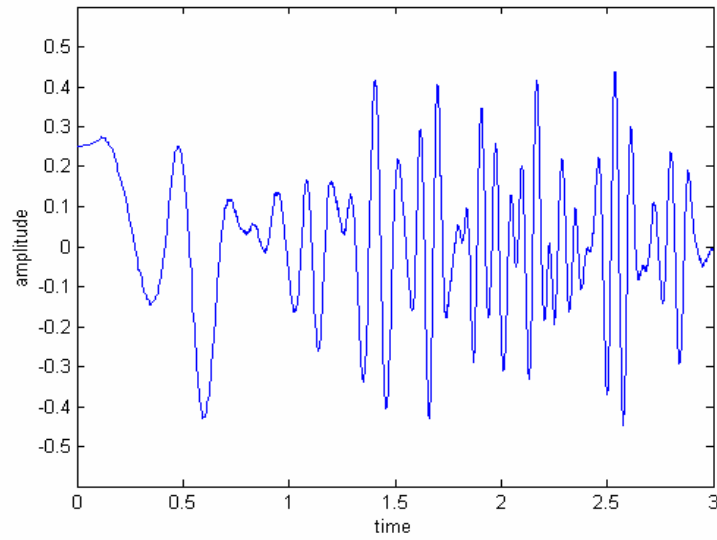


Figure 2.7 Reflected signal when the Gaussian pulses interacts with the medium

This signal is then time reversed and is then sent back into the same medium which gives us the pulses in the same sequence as we originally sent them into the medium (Fig.2.8). A threshold level can be prescribed to detect the refocused pulse. This threshold can vary depending on the application and amplitude of the original pulse. Here we can see the sequence generated after time reversal to be $\{1,0,0,1,0,1\}$ which is exactly the reverse of the input sequence. This shows the FILO property of the time reversed signal.

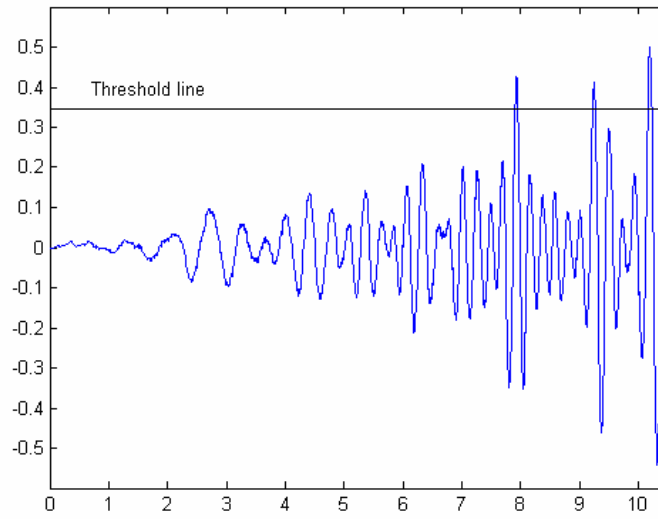


Figure 2.8 Refocused train of pulses

The method is implemented using the C language on an 896 MHz Intel Celeron-processor IBM ThinkPad. The time taken for computing the time-reversal wave for one realization using 100 layers ($N = 100$) in this method is approximately 4 min 32 sec = 272 sec.

3. FINITE DIFFERENCE TIME DOMAIN (FDTD) METHOD

3.1 INTRODUCTION

Let h and k be positive numbers. We can define a grid by grid points $(t_n, x_m) = (nk, mh)$ for arbitrary positive integers n and m . For a function v defined on the grid we write v_m^n for the value of v at the grid point (t_n, x_m) . The set of points (t_n, x_m) for a fixed value of n is called grid level n .

The basic idea of finite difference schemes is to replace derivatives by finite difference approximations. For example:

$$\begin{aligned}\partial u / \partial t (nk, mh) &= (u((n+1)k, mh) - u(nk, mh)) / k \\ &= (u((n+1)k, mh) - u((n-1)k, mh)) / (2k)\end{aligned}$$

There are various finite difference schemes for the 1-D wave equation and several are shown below:

$$(V_m^{n+1} - V_m^n) / k + a \cdot (V_{m+1}^n - V_m^n) / h = 0 \quad (3.1)$$

$$(V_m^{n+1} - V_m^n) / k + a \cdot (V_m^n - V_{m-1}^n) / h = 0 \quad (3.2)$$

$$(V_m^{n+1} - V_m^n) / k + a \cdot (V_{m+1}^n - V_{m-1}^n) / (2h) = 0 \quad (3.3)$$

$$(V_m^{n+1} - V_m^{n-1}) / (2k) + a \cdot (V_{m+1}^n - V_{m-1}^n) / (2h) = 0 \quad (3.4)$$

$$(V_m^{n+1} - \frac{1}{2}(V_{m+1}^n + V_{m-1}^n)) / k + a \cdot (V_{m+1}^n - V_{m-1}^n) / (2h) = 0 \quad (3.5)$$

where Eq(3.1) – forward-time forward-space (2,2) scheme.

Eq(3.2)– forward-time backward-space (2,2) scheme.

Eq(3.3) – forward-time central-space (2,2) scheme.

Eq(3.4) – Leapfrog (2,2) scheme.

Eq(3.5) – Lax-Friedrichs (2,2) scheme.

3.2 FORMULATION OF EQUATIONS:

We start with the 1-D wave equation:

$$\partial^2 u / \partial t^2 (x,t) - \alpha^2 \partial^2 u / \partial x^2 (x,t) = 0, \quad 0 < x < 1 \quad \text{and } t > 0$$

subject to the following boundary and initial conditions -

$$u(0,t) = u(1,t) = 0, \quad t > 0$$

$$u(x,0) = f(x), \quad 0 \leq x \leq 1$$

$$\partial u / \partial t (x,0) = g(x), \quad 0 \leq x \leq 1,$$

where α = velocity of propagation.

To set up a finite difference method, select an integer $m > 0$ and time – step size $k > 0$.

With $h=1/m$, the mesh points (x_i, t_j) are defined as:

$$x_i = ih \quad \text{for } i = 0, 1, 2, \dots, m$$

$$t_j = jk \quad \text{for } j = 0, 1, 2, \dots, N$$

At any interior mesh point (x_i, t_j) , the wave equation becomes,

$$\partial^2 u / \partial t^2 (x_i, t_j) - \alpha_i^2 \partial^2 u / \partial x^2 (x_i, t_j) = 0 \quad (3.6)$$

The Finite difference method is obtained using the center – difference equation quotient

for the second partial derivatives given by:

$$\partial^2 u / \partial t^2 (x_i, t_j) = [u(x_i, t_{j+1}) - 2u(x_i, t_j) + u(x_i, t_{j-1}))]/k^2 - k^2/12 \cdot \partial^4 u / \partial t^4 (x_i, t_j)$$

where $t_{j-1} < \mu_j < t_{j+1}$

$$\partial^2 u / \partial x^2 (x_i, t_j) = [u(x_{i+1}, t_j) - 2u(x_i, t_j) + u(x_{i-1}, t_j)] / h^2 - h^2 / 12 \cdot \partial^4 u / \partial x^4 (\xi_i, t_j)$$

where $x_{j-1} < \xi_i < x_{j+1}$

Substituting these in Eq.(3.6) ,

$$\begin{aligned} [u(x_i, t_{j+1}) - 2u(x_i, t_j) + u(x_i, t_{j-1})] / k^2 - \alpha_i^2 \cdot [u(x_{i+1}, t_j) - 2u(x_i, t_j) + u(x_{i-1}, t_j)] / h^2 \\ = 1/12 (k^2 \cdot \partial^4 u / \partial t^4 (x_i, \mu_j) - \alpha_i^2 h^2 \cdot \partial^4 u / \partial x^4 (\xi_i, t_j)) \end{aligned}$$

Neglecting the truncation error,

$$\tau_{i,j} = 1/12 (k^2 \cdot \partial^4 u / \partial t^4 (x_i, \mu_j) - \alpha_i^2 h^2 \cdot \partial^4 u / \partial x^4 (\xi_i, t_j))$$

$$\text{We have } [W_i^{j+1} - 2W_i^j + W_i^{j-1}] / k^2 - \alpha_i^2 [W_{i+1}^j - 2W_i^j + W_{i-1}^j] / h^2 = 0$$

We let $\lambda_i = \alpha_i k / h$ and hence can write the difference equation as follows :

$$W_i^{j+1} - 2W_i^j + W_i^{j-1} - \lambda_i^2 W_{i+1}^j + 2\lambda_i^2 W_i^j - \lambda_i^2 W_{i-1}^j = 0$$

and then solve for W_i^{j+1} , the most advanced time-step approximation, to obtain

$$W_i^{j+1} = 2(1 - \lambda_i^2)W_i^j + \lambda_i^2 (W_{i+1}^j + W_{i-1}^j) - W_i^{j-1} \quad (3.7)$$

This equation holds for each of $i = 1, 2, \dots, (m-1)$ and $j = 1, 2, \dots, (N-1)$

The velocities of propagation α_i for each layer 'i' can be seen in Fig 3.1. This method gets slower as we increase the number of points per layer. The least number of points we can use for each layer is 2 points per layer as we need at least 2 points for discretizing the

wave equation using the (2,2) explicit scheme. So, in order to demonstrate time-reversal, we use 2 points per layer.

As the discretization of the wave equation is second order accurate in time and second order accurate in space, this scheme is called (2,2) explicit scheme. It is called ‘explicit’ because the current value of the solution of the wave equation can be explicitly obtained from its previous values.

3.3 BOUNDARY CONDITIONS AND HIGHER ORDER ACCURATE SCHEMES

Our domain for demonstrating the time reversal is the interval [0,1]. The scatterer is located between 0.5 and 0.6 in this space with the Gaussian pulse initially to the left of the scatterer. We assume that the signal does not reach the boundaries of the domain. Thus, in this case, the wave propagation can be subject to the following boundary conditions:

$$W_0^j = W_m^j = 0 \quad j = 1, 2, \dots, N$$

Equation (3.7) is the (2,2) explicit scheme and requires a stencil of 3 mesh points, one on each side of the mesh point on which the calculation is to be done. We can also have higher order accurate schemes for the second order equations. One such scheme is the second order in time and fourth order in space ((2,4) scheme). This can be written as follows:

$$[W_i^{j+1} - 2W_i^j + W_i^{j-1}]/k^2 = \alpha_i^2 [-W_{i+2}^j + 16W_{i+1}^j - 30W_i^j + 16W_{i-1}^j - W_{i-2}^j]/12h^2$$

We let $\lambda_i = \alpha_i k/h$ and hence can write the difference equation as follows :

$$W_i^{j+1} = 2W_i^j - W_i^{j-1} + (\lambda_i^2/12)(-W_{i+2}^j + 16W_{i+1}^j - 30W_i^j + 16W_{i-1}^j - W_{i-2}^j) \quad (3.8)$$

This equation requires a stencil of 5 mesh points, two on each side of the mesh point on which the calculation is to be done. This method gives us more accurate results compared to the (2,2) scheme but increases the computational complexity.

3.4 ALGORITHM

The algorithm used for implementing time reversal using the FDTD method employs the (2,4) scheme discussed above. As this scheme requires 2 mesh points on each side of the mesh point on which the calculation is being done, the second and the second last mesh point uses the (2,2) scheme to evaluate values at those mesh points.

We approximate W_i^j to $u(x_i, t_j)$ for each $i = 0, 1, 2, \dots, m$ & $j = 0, 1, 2, \dots, N$ and thereafter proceed to the following steps of the algorithm:

Step 1: Set $h = l/m$

$$k = T/N$$

$$\lambda = k\alpha/h$$

where l = Endpoint, T = Maximum time, α = Constant and m, N = Integers

Step 2: For $j = 1, 2, \dots, N$, $W_0^j = W_m^j = 0$

Step 3: Set $W_0^0 = f(0)$

$$W_m^0 = f(l)$$

Step 4: For $i = 1, 2, \dots, m-1$ (Initialize for $t=0$ & $t=k$)

Set $W_i^0 = f(ih)$

$$W_i^1 = (1 - \lambda^2) f(ih) + \lambda^2/12 [f((i+1)h) + f((i-1)h)] + k g(ih)$$

Step 5: For $j = 1, 2, \dots, N-1$

For $i = 1, 2, \dots, m-1$

if $i = 1$ or $i = m-1$

$$\text{Set } W_i^{j+1} = 2(1 - \lambda^2)W_i^j + \lambda^2 (W_{i+1}^j + W_{i-1}^j) - W_i^{j-1}$$

else

$$\text{Set } W_i^{j+1} = 2W_i^j - W_i^{j-1} + (\lambda^2/12)(-W_{i+2}^j + 16W_{i+1}^j - 30W_i^j$$

$$+ 16W_{i-1}^j - W_{i-2}^j)$$

Step 6: For $j = 0, 1, 2, \dots, N$

Set $t = jk$

For $i = 0, 1, 2, \dots, m$

Set $x = ih$

OUTPUT = (x, t, W_i^j)

Step 7: END

3.5 RESULTS

The implementation of time reversal in 1-D is done in accordance with the algorithm in the previous section. We create a random complex medium using the random number generator to determine the velocities in various layers of the medium. All the computations are done and results presented using MATLAB 5 on an 896 MHz Intel Celeron-processor IBM ThinkPad. The medium can be seen in Fig 3.1.

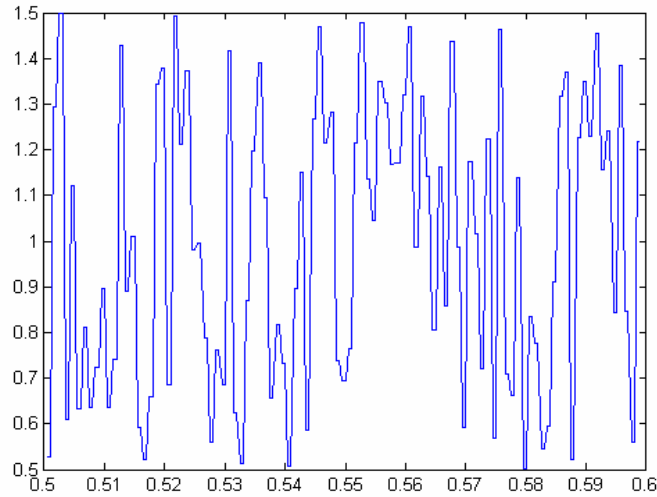


Figure 3.1 Distribution of the velocity of propagation of the random medium

For implementing time reversal using this method, we can start with any pulse. Here the pulse used is a Gaussian pulse defined by the equation:

$$f(t) = - (t/\sqrt{\varepsilon}) * \exp(-t^2/2*\varepsilon)$$

which can be viewed in Fig 3.2.

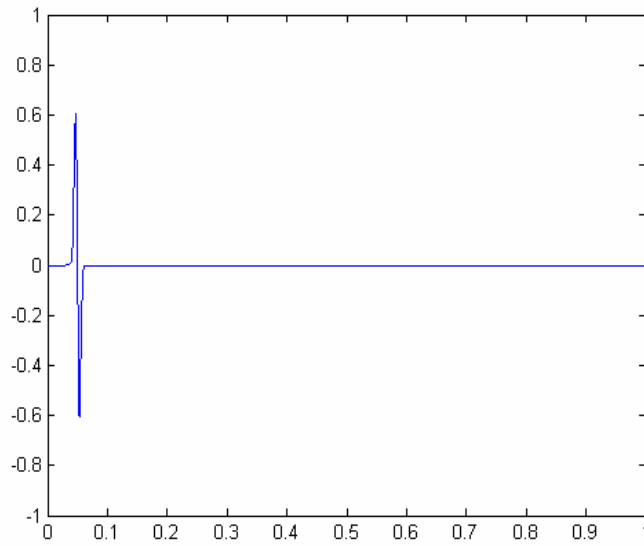


Figure 3.2 Initial Gaussian pulse

This pulse, when propagated through the random complex media, gives rise to a reflected signal and a transmitted (refracted) signal. This can be seen in the Fig 3.3.

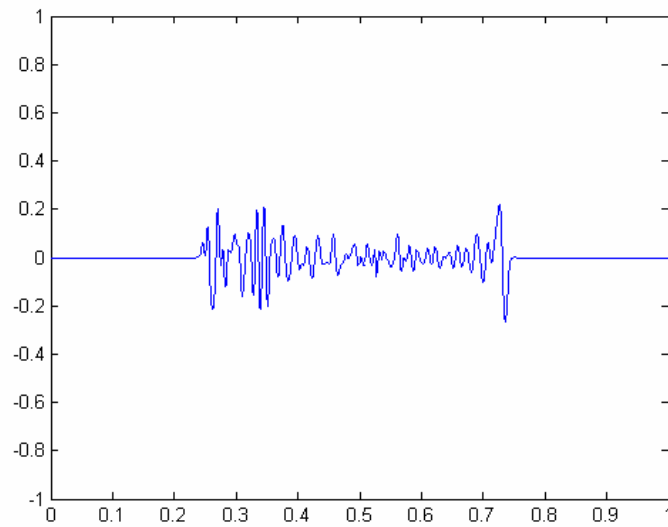


Figure 3.3 Reflected and transmitted signal when the pulse interacts with medium

To demonstrate time reversal of the reflected signal, the reflected wave is then taken and sent through the same complex random medium after time reversal i.e. the part of the signal that comes out first will go in last into the medium (LIFO). This gives rise to pulse refocusing and we can see a pulse which is of the same shape as the original pulse, and reduced amplitude because we are storing only the reflected wave and also due to some loss of energy due to propagation. The refocused pulse can be seen in the Fig 3.4.

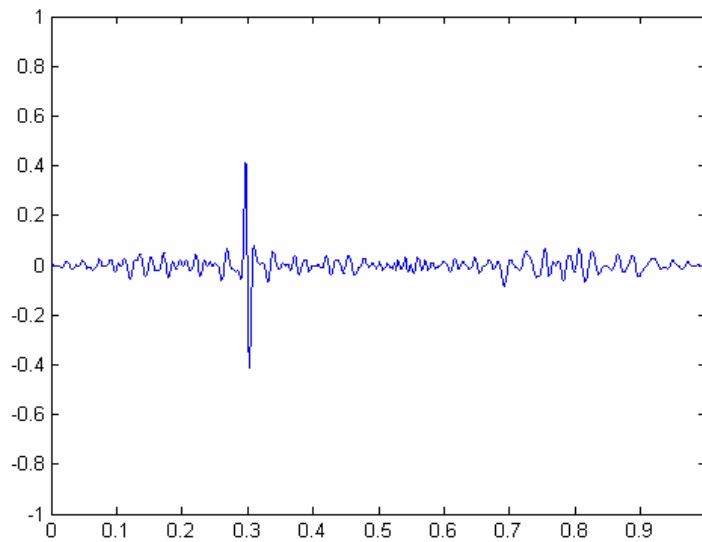


Figure 3.4 Refocused pulse

Fig. 3.5 is the magnified view of the refocused pulse. This can be used to study characteristics of the refocused pulse and the amplitude of the refocused pulse can be used in medical applications and underground object detection.

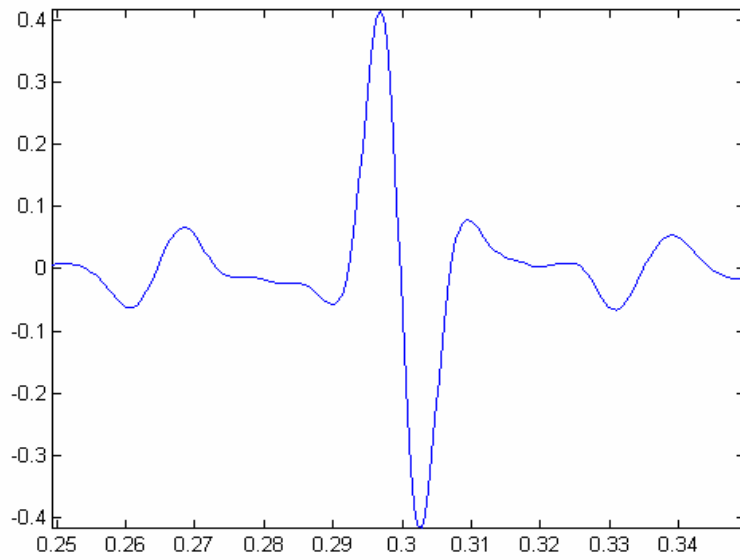


Figure 3.5 Magnified view of the refocused pulse

3.6 DIFFERENT REALIZATIONS USING VARIOUS RANDOM MEDIA

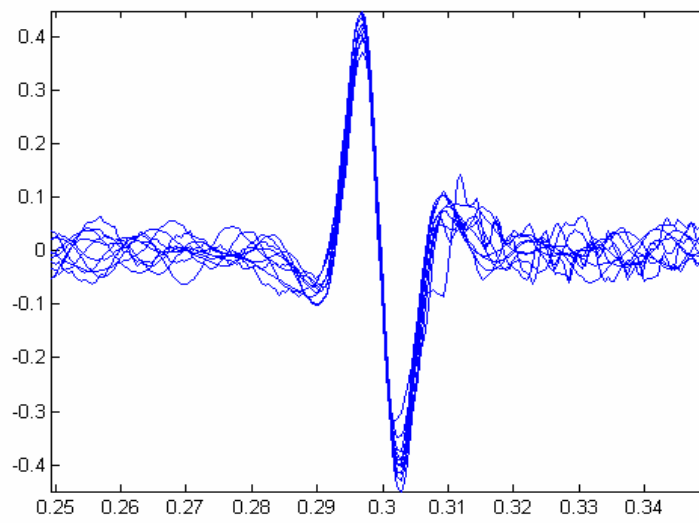


Figure 3.6 10 Random realizations of the refocused pulse

Fig 3.6 shows the refocused pulse for 10 different realizations using different complex media each having $N=100$ layers and velocities of propagation distributed uniformly between 0.5 and 1.5. It can be seen clearly that for each of the realizations, the position and the amplitude of the pulse is independent of the way the velocities in the complex media are assigned. Only the low-amplitude coda around the pulse is different for different random complex medias. Hence we can say that the pulse refocuses in a manner that is self-averaging with respect to random realizations of wave speed in the component layers of the random complex media.

3.7 NUMERICAL CONVERGENCE AND TIME CONSIDERATIONS

The most basic property that a scheme must have in order to be useful is that its solutions approximate the solution of the corresponding partial differential equation and that the approximation improves as the grid spacing h and k , tend to zero. We call such a scheme a convergent scheme. The grid spacing will tend to zero as we increase the number of points per layer for each of the layers. In our (2,4) explicit scheme, as we increase the number of points per layer, the refocused pulse amplitude converges to some limiting amplitude and use this as a measure of the extent to which the method has numerically converged. The execution time to achieve the refocused pulse for one realization having 100 layers and 2 points per layer is approximately 15 min 55 sec = 955 sec on MATLAB

5 using 896 MHz Intel Celeron-processor IBM ThinkPad. This makes it clear that the FDTD method is time consuming and hence makes parametric analysis tedious.

4. BOUNDARY INTEGRAL METHOD

4.1 INTRODUCTION

The boundary integral scheme is formulated in the frequency domain. This method is based on Green's functions and is very efficient in dealing with problems in 1-D involving interface conditions. We start with the definition of the Fourier Transform followed by an explanation of the method which involves the Helmholtz equation. We define the Fourier Transform as follows:

$$\text{Fourier Transform: } \hat{u}(\omega) \equiv \int_{-\infty}^{\infty} e^{i\omega t} u(x, t) dt$$

Using this definition, we write the wave equation:

$$\partial^2 u / \partial t^2 (x, t) - \alpha^2 \partial^2 u / \partial x^2 (x, t) = 0$$

in the frequency domain by taking Fourier Transform of each of its terms. The representation in the frequency domain reduces to Helmholtz equation:

Helmholtz Equation : $(-\infty < \omega < \infty)$

$$\partial_x^2 \hat{u}(x, \omega) + k_j^2 \hat{u}(x, \omega) = 0, \quad x \in \Omega_j \quad (k_j = \omega / c) \quad (4.1)$$

$$\partial_x^2 \hat{u}(x, \omega) + k^2 \hat{u}(x, \omega) = 0, \quad x \in (-\infty, a_0) \cup (a_N, \infty) \quad (k = \omega / c) \quad (4.2)$$

where layer 'j' can be represented by $\Omega_j = (a_j, a_{j+1})$ and a_j and a_{j+1} represents the two boundaries of the layer 'j'.

Now we introduce Green's function for each domain that satisfy:

Green's Functions for each subdomain : $(-\infty < \omega < \infty)$

$$\partial_x^2 \hat{H}^j(x, y, \omega) + k_j^2 \hat{H}^j(x, y, \omega) = \delta(x - y), \quad x, y \in \Omega_j \quad (4.3)$$

$$\partial_x^2 \hat{H}(x, y, \omega) + k^2 \hat{H}(x, y, \omega) = \delta(x - y), \quad x, y \in (-\infty, a_0) \cup (a_N, \infty) \quad (4.4)$$

where $\delta(x)$ is the Dirac delta function. For an incident wave that propagates from left to right, the Green's function that satisfy the above two equations are respectively:

$$\hat{H}^j(x, y, \omega) = \frac{e^{ik_j|x-y|}}{2ik_j}, \quad x, y \in \Omega_j$$

$$\hat{H}(x, y, \omega) = \frac{e^{ik|x-y|}}{2ik}, \quad x, y \in (-\infty, a_0) \cup (a_N, \infty)$$

4.2 ASSEMBLY OF THE SYSTEM OF EQUATIONS

We multiply Equation (4.3) by $\hat{u}(x)$ and (4.2) by $\hat{H}^j(x, y)$ and then subtract one equation from the other. Integrating the above expression along the region between the two interfaces would give us the expression at any point.

For $y \in (a_j, a_{j+1})$:

$$\int_{a_j}^{a_{j+1}} \hat{u}(x) \delta(x - y) dx = \int_{a_j}^{a_{j+1}} \partial_x^2 \hat{H}^j(x, y) \hat{u}(x) dx - \int_{a_j}^{a_{j+1}} \hat{H}^j(x, y) \partial_x^2 \hat{u}(x) dx$$

Using the filtering property of the Dirac delta function and integration by parts, we get:

$$\begin{aligned}\hat{u}(y) = & \partial_x \hat{H}^j(a_{j+1}, y) \hat{u}(a_{j+1}) - \partial_x \hat{H}^j(a_j, y) \hat{u}(a_j) \\ & - \hat{H}^j(a_{j+1}, y) \partial_x \hat{u}(a_{j+1}) + \hat{H}^j(a_j, y) \partial_x \hat{u}(a_j)\end{aligned}$$

We obtain a closed system of linear algebraic equations for the unknown quantities on the interfaces by taking the limit as the interior point y approaches the end points of each interval (a_j, a_{j+1}) .

$$\begin{aligned}y \rightarrow a_j^+ \Rightarrow \hat{u}(a_j) = & \partial_x \hat{H}^j(a_{j+1}, a_j^+) \hat{u}(a_{j+1}) - \partial_x \hat{H}^j(a_j, a_j^+) \hat{u}(a_j) \\ & - \hat{H}^j(a_{j+1}, a_j^+) \partial_x \hat{u}(a_{j+1}) + \hat{H}^j(a_j, a_j^+) \partial_x \hat{u}(a_j) \\ y \rightarrow a_{j+1}^- \Rightarrow \hat{u}(a_{j+1}) = & \partial_x \hat{H}^j(a_{j+1}, a_{j+1}^-) \hat{u}(a_{j+1}) - \partial_x \hat{H}^j(a_j, a_{j+1}^-) \hat{u}(a_j) \\ & - \hat{H}^j(a_{j+1}, a_{j+1}^-) \partial_x \hat{u}(a_{j+1}) + \hat{H}^j(a_j, a_{j+1}^-) \partial_x \hat{u}(a_j)\end{aligned}$$

These two equations comprise $2N$ equations in the $2N+2$ unknowns consisting of the values of \hat{u} and $\partial_x \hat{u}$ on the interfaces located at $y=a_0, \dots, y=a_N$ known as the Layer Interface Equations.

Layer Interface Equations : $j = 0, 1, \dots, N-1$

$$\frac{1}{2} \hat{u}(a_j) - \frac{1}{2ik_j} \partial_x \hat{u}(a_j) = \partial_x \hat{H}^j(a_{j+1}, a_j^+) \hat{u}(a_{j+1}) - \hat{H}^j(a_{j+1}, a_j^+) \partial_x \hat{u}(a_{j+1})$$

$$\frac{1}{2} \hat{u}(a_{j+1}) + \frac{1}{2ik_j} \partial_x \hat{u}(a_{j+1}) = -\partial_x \hat{H}^j(a_j, a_{j+1}^-) \hat{u}(a_j) + \hat{H}^j(a_j, a_{j+1}^-) \partial_x \hat{u}(a_j)$$

Two additional equations are obtained by performing a similar limit analysis on the intervals $(-\infty, a_0)$ and (a_N, ∞) and hence complete the formulation of a closed system of linear algebraic equations for the interface unknowns.

Left end of scatterer : $y \in (-L, a_0)$. Let $L \rightarrow \infty, y \rightarrow a_0^-$:

$$\frac{1}{2}\hat{u}(a_0) + \frac{1}{2ik}\partial_x \hat{u}(a_0) = e^{ika_0}$$

Right end of scatterer : $y \in (a_N, L)$. Let $L \rightarrow \infty, y \rightarrow a_N^+$:

$$\frac{1}{2}\hat{u}(a_N) - \frac{1}{2ik}\partial_x \hat{u}(a_N) = 0$$

Now we can use this method for a specific incident pulse. We consider a Gaussian pulse centered at $y=y_0$ and having velocity c with variance δ .

$$\text{Incident pulse : } f(y - y_0 - ct) = \frac{1}{\sqrt{2\pi}\delta} e^{-(y-y_0-ct)^2/(2\delta^2)}$$

The incident pulse used for the simulation is the first derivative of the Gaussian pulse. The following equation gives the formula for the refocused pulse after time reversal for a incident pulse (derivative of Gaussian) centered at y_0 with variance $= \delta$.

Reflected wave for analysis of time - reversal refocusing

$$\begin{aligned} \hat{u}_{\text{tr}}^{\text{ref}}(\omega) &= \frac{1}{2\pi c} (\hat{R}(\omega/c) e^{-i\omega y/c} + e^{i\omega y/c}) e^{i\omega(t_0 + (y-y^*)/c)} \\ &\times \int_{-\infty}^{\infty} e^{-\delta^2 \tilde{\omega}^2 / (2c^2)} e^{-i\tilde{\omega}(y-y^*)/c} e^{i\tilde{\omega}(t^* + y_0/c)} \left(e^{i\tilde{\omega}y/c} \hat{R}(\tilde{\omega}/c) + e^{-i\tilde{\omega}y/c} \right) \frac{e^{i(\tilde{\omega}-\omega)t_0} - 1}{i(\tilde{\omega}-\omega)} d\tilde{\omega} \end{aligned}$$

4.3 PULSE REFOCUSING AND RANDOM REALIZATIONS

To get the pulse refocusing via time-reversal in 1-D using this method, we can start with a Gaussian derivative pulse defined by the equation:

$$f(t) = - (t/\sqrt{\varepsilon}) * \exp(-t^2/2*\varepsilon)$$

and shown in Fig. 3.2. We then formulate the set of equations discussed in the previous section to get the refocusing of the pulse.

Here we set the number of layers, $N=100$, the length of sampling interval $t_0 = 3.0$ and variance of the pulse $\delta = 0.01$. The refocused pulse is shown in the Fig 4.1 below.

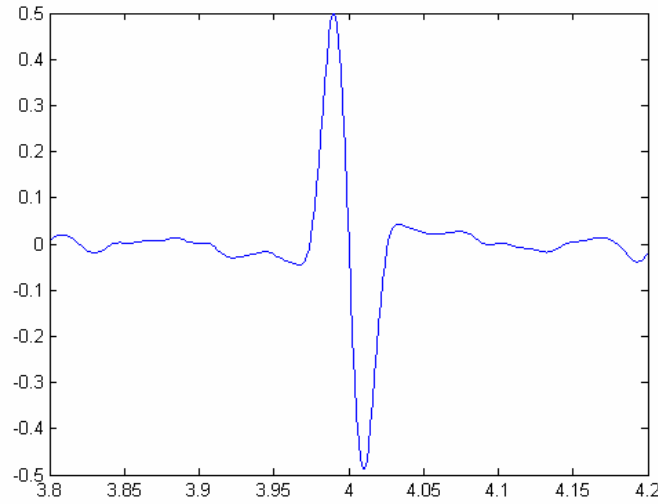


Figure 4.1 Refocused pulse

Implementing Time reversal using multiple realizations of the medium and plotting results on the same axes helps us conclude that the shape of the refocused pulse is independent of the realization of the medium.

We can demonstrate this self-averaging property by taking 10 different realizations for $N=100$ and velocities of propagation generated using a random number generator. All the computations are done and results presented using MATLAB 5 on an 896 MHz Intel Celeron-processor IBM ThinkPad

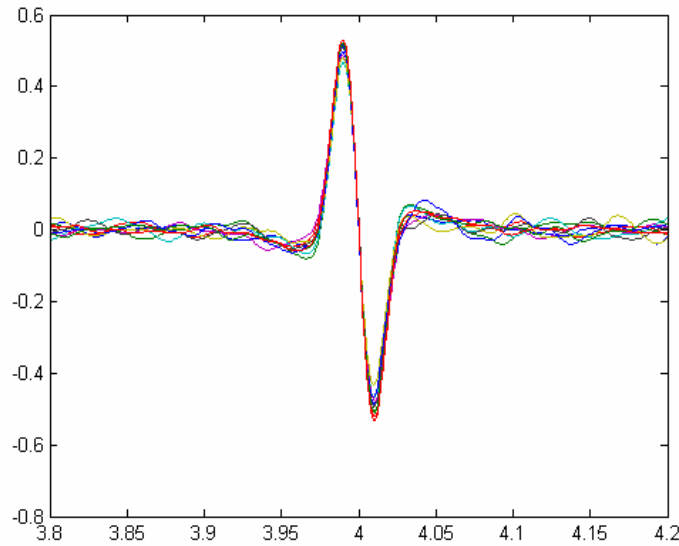


Figure 4.2 10 Random realizations of the refocused pulse

4.4 EFFECT OF INCREASING THE NUMBER OF LAYERS:

Here we illustrate the refocusing of the time-reversed pulse as the number of layers N in the scatterer is increased. For each N , we computed the time-reversed pulse for 10 different realizations of the scatterer. As more layers are added to the scatterer, the separation between the scales of the layer width and typical pulse wavelength increases.

In this regime, the self-averaging property of the refocused pulse becomes more pronounced which can be seen by comparing the figures below. The characteristic wavelength of the refocused pulse is on the same scale as the original incident pulse. As N increases we can have a direct comparison of the numerical simulations to the theoretical results ($N \rightarrow \infty$).

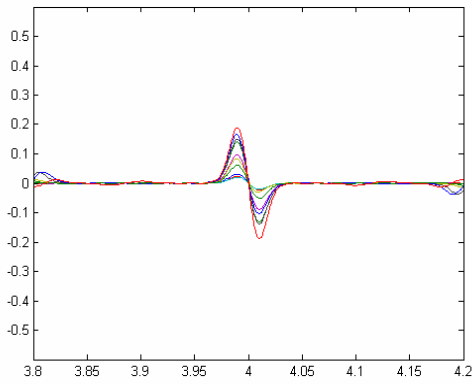


Figure 4.3 10 Random realizations of the refocused pulse ($N=5$)

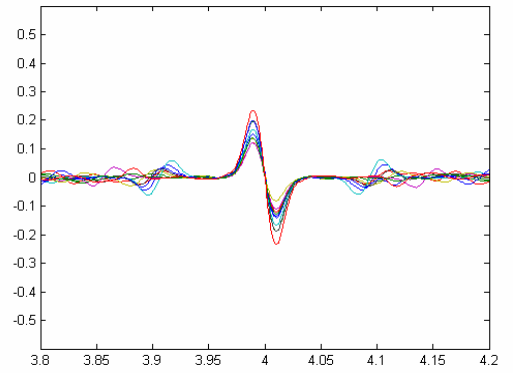


Figure 4.4 10 Random realizations of the refocused pulse ($N=10$)

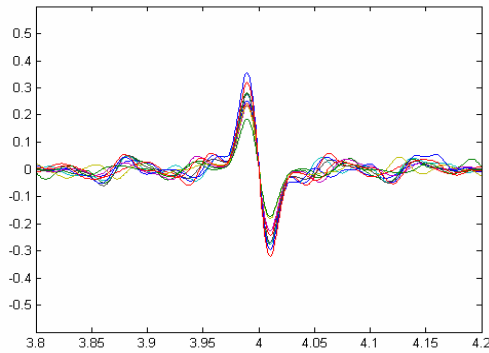


Figure 4.5 10 Random realizations of the refocused pulse ($N=20$)

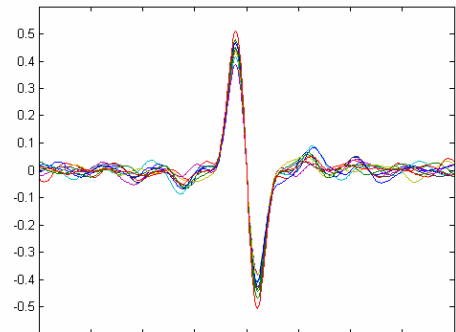


Figure 4.6 10 Random realizations of the refocused pulse ($N=50$)

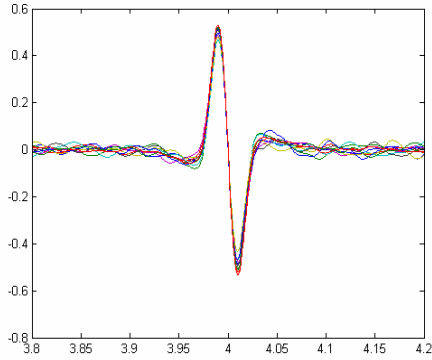


Figure 4.7 10 Random realizations of the refocused pulse (N=100)

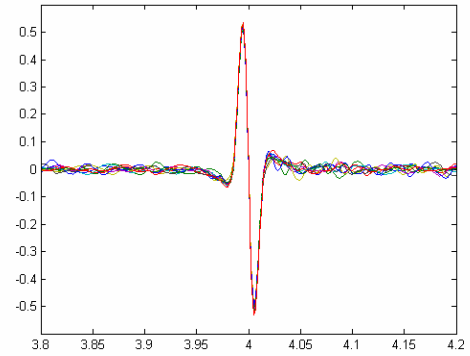


Figure 4.8 10 Random realizations of the refocused pulse (N=300)

Table 1 below shows the comparison of the standard deviations of the amplitudes of the refocused pulse for 25 different realizations with number of layers $N = 100, 300$ and 500 .

Table 1: Study of effect of increasing the number of layers on the pulse amplitude for 25 different realizations

Number of Layers	100	300	500
Mean	0.5290	0.5088	0.4837
Std Deviation	0.0391	0.0201	0.0154

We observe that as we increase the number of layers N , the variation (standard deviation) in the amplitude of the refocused pulse reduces significantly and tends to some limiting theoretical value.

4.5 VERIFICATION OF THE THEORETICAL FORMULA:

Time reversal in 1-D has been implemented using 3 different methods and it is seen that the self-averaging property can be demonstrated using each of those methods. Here will be compare the numerical results achieved using the Boundary Integral Method to the theoretical formula for the time reversed pulse. We start the analysis with our incident pulse given by:

$$\begin{aligned} f(t) &= d/dt(\exp(-t^2/2)) \\ &= t \cdot \exp(-t^2/2) \end{aligned}$$

If our velocities of propagation are defined for different layers as:

$$1/c^2 = 1 + \mu(x)$$

where $\mu(x) = U(-0.8, 0.8)$

Then we calculate ‘ α ’ called the integrated correlation as follows:

$$\begin{aligned} \alpha &= \int_0^\infty E[\mu(0)\mu(x)]dx \\ &= \int_{-0.8}^{0.8} x^2 dx \\ &= [x^3/3]_{-0.8}^{0.8} \\ &= 128/375 \end{aligned}$$

Once you have the integrated correlation, the refocused pulse is given by:

$$f_{TR}(t) = (f * H_{t0})(t)$$

where $H_{t_0'}(t)$ = some kernel function

$$=F^{-1}[\Lambda(w, \cdot) * G_{t_0'}(\cdot)](0)$$

with $\Lambda(w, \cdot) = \alpha w^2 / (1 + w^2 \alpha t)^2$ and $G_{t_0'}(\cdot) =$ cutoff function between 0 to t_0' .

Using these two expressions we calculate the kernel function.

$$\begin{aligned} [\Lambda(w, \cdot) * G_{t_0'}(\cdot)](0) &= \int_0^{\infty} \Lambda(w, \tau) G_{t_0'}(\tau) d\tau \\ &= \int_0^{t_0'} \Lambda(w, \tau) d\tau \\ &= \int_0^{t_0'} \alpha w^2 / (1 + w^2 \alpha \tau)^2 d\tau \\ &= \alpha w^2 t_0' / (1 + w^2 \alpha t_0') \end{aligned}$$

Hence, $f_{TR}(t) = (f * H_{t_0'})(t)$

$$\begin{aligned} &= F^{-1} [f(w) \cdot H_{t_0'}(w)] \\ &= 1/2\pi \int e^{-iwt} \cdot f(w) \cdot \alpha w^2 t_0' / (1 + w^2 \alpha t_0') dw \end{aligned}$$

where $f(w) = F[f(t)] = -iw \exp(-w^2/2)$

$$\text{Therefore } f_{TR}(t) = 1/2\pi \int e^{-iwt} \cdot (-iw \cdot e^{-w^2/2}) \cdot \alpha w^2 t_0' / (1 + w^2 \alpha t_0') dw$$

This is the final pulse which we get after time reversal. This is compared with the numerical results for varying number of layers and results show that for sufficiently large number of layers (e.g. $N = 100$), the numerical results approach the theoretical values.

In the Fig 4.9 the dotted line indicates the theoretical time reversed pulse and the solid lines indicate numerical results for the mean curve over 10 different realizations with varying number of layers. It can be seen clearly that as we increase the number of layers N , the numerical result approaches the theoretical formula.

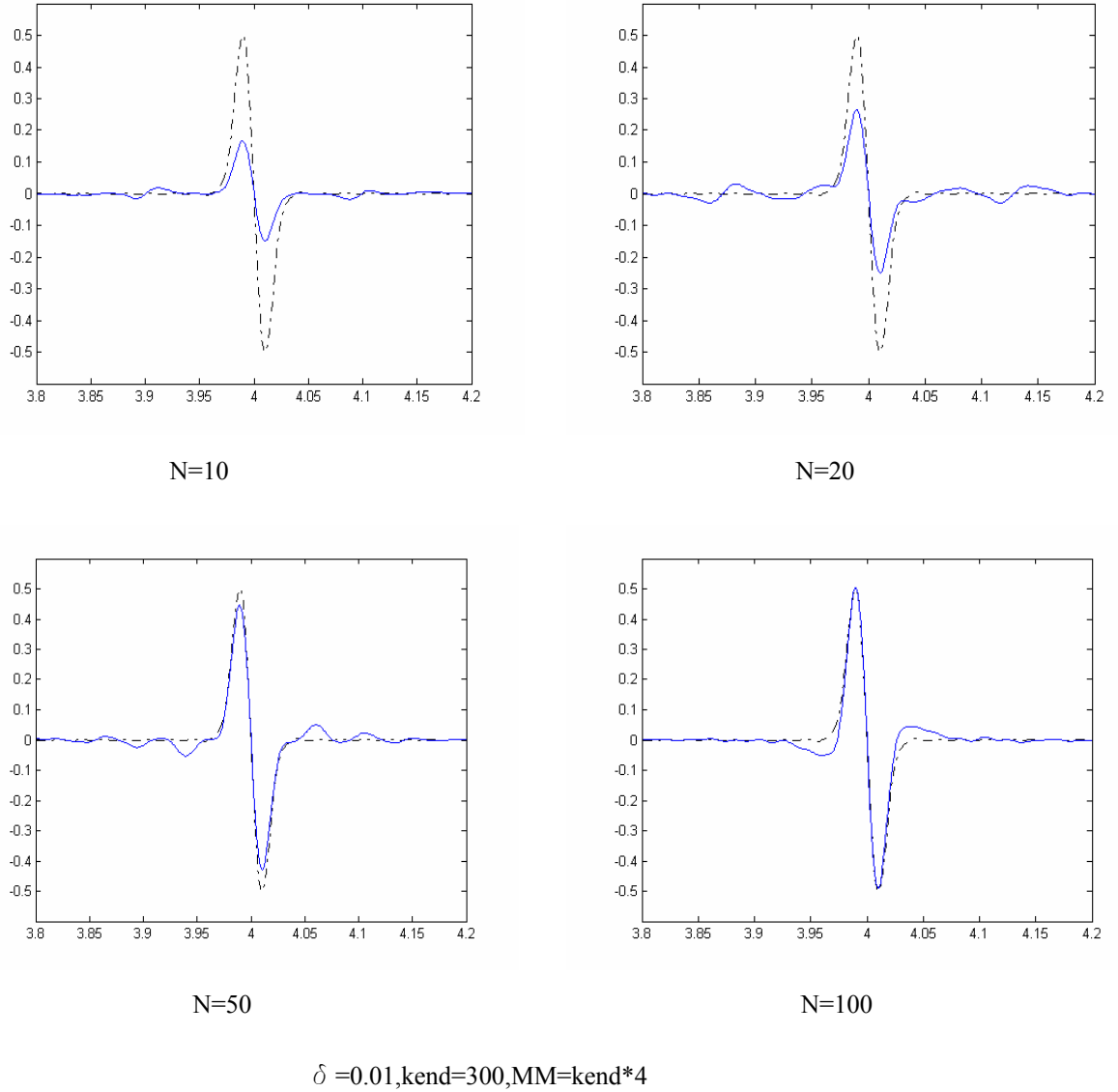


Figure 4.9 Verification of theoretical formula for different number of layers

Table 2 gives a very clear picture that while addressing a problem in 1-D which is linear in nature, the Boundary Integral Method is preferable to the other two methods. However, if we address problems in 2-D and 3-D or problems having a non-linear property then the FDTD method may be necessary.

Table 2: Comparative Study of the three methods in terms of speed and accuracy.

	Transfer Matrix Method	Finite Difference Time Domain Method	Boundary Integral Multiple Method
Principle	Convolution layer by layer.	Discretize the wave equation using the finite difference schemes.	Uses the Green's function and Helmholtz equation.
Time for one realization (100 layers)	4 min 32 sec = 272 sec	15 min 55 sec = 955 sec (2 points per layer)	80 sec
Type of problems that can be solved	1- D problems can be easily implemented. However, the method may not be a practical approach for higher dimension problems.	This method can be used for 1- D linear problems. Also it can be extended to higher dimensions as well as non-linear problems using the same approach.	This method is preferred to the other two methods for 1-D linear problems. However, it can't be used for non-linear problems due to the use of Green's function which is itself linear in nature.

5. DETECTION OF A BURIED CAVITY VIA TIME-REVERSAL

5.1 HYPOTHESIS

After having implemented time-reversal in 1-D successfully using the Boundary Integral Method, its potential for being used in various applications such as detection of a cavity/object buried in a random layered scatterer is now analyzed. We hypothesize that time-reversal detection can be evaluated by comparing the amplitude of the time-reversed pulse for a realization of the layered medium to the amplitude of the time-reversed pulse for the same realization of the layered medium with a hollow cavity. It will be seen that the amplitude of the time-reversed pulse can be used as a measure for detection of a cavity buried in a random layered scatterer. Statistics of the time reversed pulse amplitude for several cases is also shown which helps in making some useful deductions about the presence and size of the target to be detected.

5.2 EXPERIMENTS

Numerical simulations were conducted on the scales $N = 100$, $\delta = 0.01$ with the wave speed of the layers varying randomly according to $c_j = 1 + \eta_j$, where (η_j) is independent and identically distributed on the interval $(-0.8, 0.8)$. In this regime, the time required for

numerical convergence of the refocused pulse for a single realization of the scatterer was roughly 80 seconds. While the chosen scales are relatively coarse, our simulations illustrate the potential for using the self-averaging property of the time-reversed pulse in detection of a buried cavity. The cavity is introduced by removing $L/2$ layers on either side of a specified location $y = y_c$ within the scatterer. To illustrate the effect of a cavity on the amplitude of the refocused pulse, a sample realization in the case where $L = 50$, $y_c = 0.5$, $t^* = 2.0$, $t_0 = 3.0$ is shown in Fig 5.1. We observe that the pulse amplitude drops in the presence of a buried cavity (Figure 5.1). This drop in the amplitude of the refocused pulse suggests presence of a buried object/cavity in the medium.

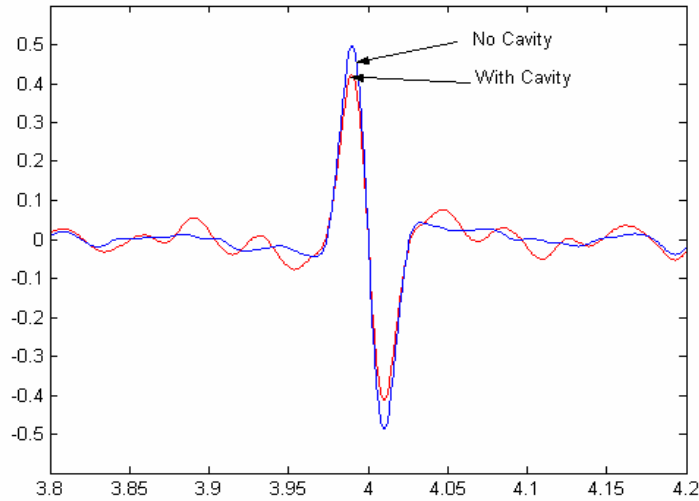


Figure 5.1 Comparison of pulse amplitude with and without cavity

The amplitudes of the pulse with and without cavity are compared for 50 different realizations (Figure 5.2). We can see that the amplitude of the pulse without cavity almost always remains above the amplitude of the pulse with cavity (Figure 5.2).

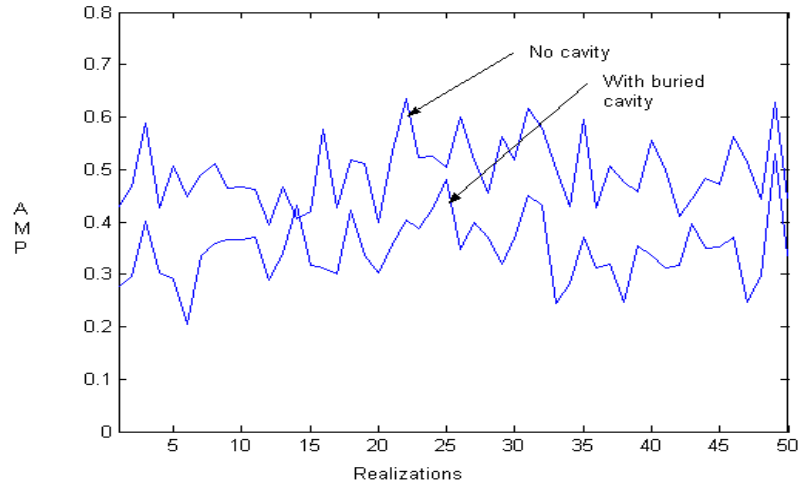


Figure 5.2 Comparison of pulse amplitudes with and without cavity for 50 realizations

We consider a detailed analysis for using the refocused pulse as a measure to detect buried targets. We observe that the amplitude of the refocused pulse is a good indicator and shows a promise for detecting buried objects/cavity.

As a specific detection measure of the time-reversed pulse, we choose the signed percentage difference between the two pulse amplitudes:

$$\text{(i.e. } [(\text{no cavity}) - (\text{cavity})] / (\text{no cavity}) \text{)}$$

For $y_c = 0.5$, $t^* = 2.0$ and $t_0 = 3.0$, this measure is plotted for 50 realizations in the cases of a relatively large cavity $L = 50$ (Figure 5.3).

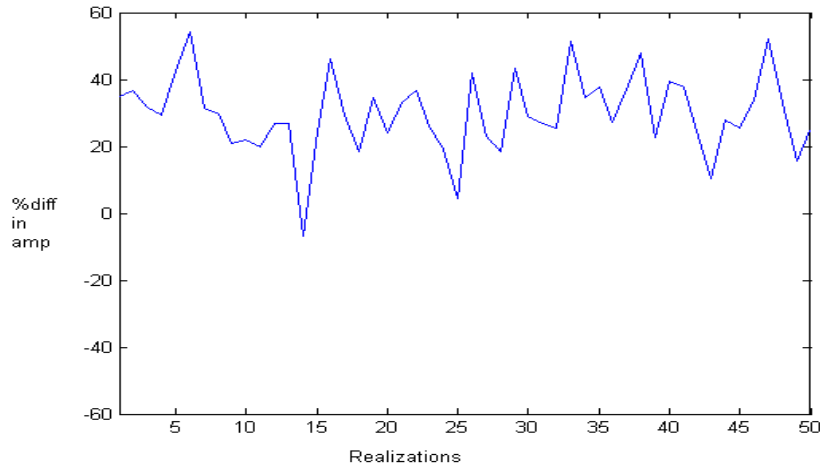
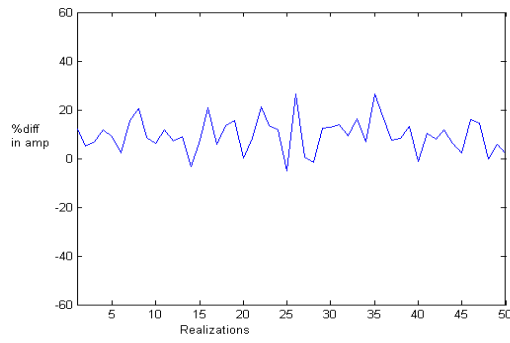


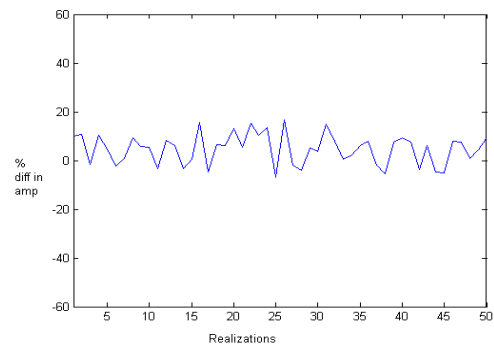
Figure 5.3 % difference of the amplitudes with and without cavity ($L=50$) for 50 realizations

The values of the signed percentage difference can help us deduce the size of the object. To study this, we can compare the result in Fig 5.3 with results of various other values of L . The Fig 5.4 below shows the signed percentage difference for $L=20$, 10 and 4.

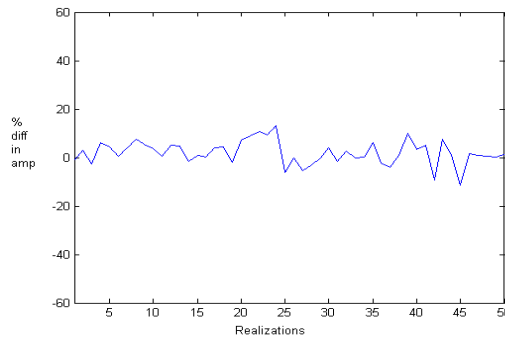
We can deduce the size of the buried object/cavity using the results in the figure above. The size of the object/cavity appears to increase with the value of the percentage difference.



% difference for L=20



% difference for L=10



% difference for L=4

Figure 5.4 % difference of the amplitudes (L=20, 10, 4) for 50 realizations

5.3 STATISTICAL ANALYSIS OF TIME REVERSED PULSE AMPLITUDE:

Statistics of this detection measure indicate the mean percentage difference increase with L . On the scales considered, these values indicate that this detection measure is a good indicator of the presence of a relatively large buried cavity. The values of the time-reversed pulse amplitude for several cases are shown in Table 3.

Table 3: Statistics of time-reversed pulse amplitude for different size of object/cavity for number of layers $N=100$. Mean values are reported with standard deviations in parentheses.

Case	t_0	L	y_c	Amplitude (no cavity)	Amplitude (cavity)	Signed % difference
1	3.0	50	0.5	0.479 (0.055)	0.320 (0.050)	33.37% (5.75%)
2	3.0	20	0.5	0.479 (0.055)	0.432 (0.049)	9.84% (5.55%)
3	3.0	10	0.5	0.479 (0.055)	0.455 (0.051)	5.31% (4.72%)
4	3.0	4	0.5	0.479 (0.055)	0.465 (0.053)	3.11% (4.82%)

The values of the signed percentage difference show promise for using time-reversal to detect the size of a buried cavity. We can see that the percentage difference decreases as we reduce the value of L . Hence, the percentage difference in the amplitudes of the refocused pulse with and without the cavity/object is a good indicator of the size of the object/cavity.

Table 4 indicates the extent to which the detection measure can indicate the depth of a buried cavity when $L=20$ and $y_c = 0.67$. By increasing t_0 when $t^* = 2.0$, we simulated the effects of gradually increasing the duration of the recording window for the reflected signal that is time-reversed and re-introduced into the scatterer.

Table 4: Statistics of time-reversed pulse amplitude to analyze the extent to which the detection measure can indicate the depth of buried cavity for $N=100$. Mean values are reported with standard deviations in parentheses.

Case	t_0	L	y_c	Amplitude (no cavity)	Amplitude (cavity)	Signed % difference
1	0.8	20	0.67	0.260 (0.066)	0.258 (0.062)	0.11% (1.70%)
2	1.0	20	0.67	0.299 (0.070)	0.300 (0.068)	0.11% (0.92%)
3	1.2	20	0.67	0.330 (0.075)	0.327 (0.072)	0.78% (2.34%)
4	1.5	20	0.67	0.376 (0.066)	0.345 (0.078)	8.99% (8.24%)
5	2.0	20	0.67	0.435 (0.055)	0.390 (0.065)	10.30% (8.00%)
6	3.0	20	0.67	0.480 (0.060)	0.425 (0.065)	10.52% (7.99%)

For smaller values of t_0 (Cases 1-3), we observe that the detection measure does not indicate any significant drop in pulse amplitude in the presence of the buried cavity. As t_0 is increased, the percentage difference increased when the time-reversal window incorporates portions of the reflected signal that correlates to the depth in the scatterer at which the cavity is buried (Cases 4-6). More extensive studies are required to determine specific relations between the critical value of the recording duration t_0 for the reflected signal and the depth y_c of the buried cavity.

For the layer resolution considered in this study ($N = 100$), the amplitude of the time-reversed pulse is a good indicator of the presence or absence of a relatively large buried cavity (of length L). The time-reversed pulse also shows promise as an indicator of cavity size and depth within the scatterer, although more extensive parametric studies are required.

6. CONCLUSIONS AND FUTURE WORK

Time reversal of waves propagating in random media was successfully implemented using the three different methods. In particular, the results of 1-D time reversal using the Boundary Integral Method was shown to be more precise and faster compared to Finite Difference Time Domain Method and the Transfer Matrix Method. Furthermore, it is also shown that Time reversal mirrors of waves propagating in random media shows promise as a potential candidate for underground or buried object / cavity detection using the amplitude of the refocused pulse as an indicator. This principle can be extended for mine-detection purpose to detect the presence of all individual mines.

Here time reversal is implemented in one spatial domain. This method can be extended to 2-D and 3-D cases and hence become useful for more practical applications. Future work would also include conducting a more extensive set of simulations on finer scales. More detailed simulations of the detection inverse problem can be studied on finer scales by increasing N by at least one order of magnitude. Better extensive studies are required to determine specific relations between the critical value of the recording duration t_0 for the reflected signal and the depth y_c of the buried cavity. Scaling parameters including the characteristic pulse wavelength δ , sampling duration t_0 and sampling time t^* can be optimized to enhance the self-averaging properties of time-reversal in the context of detection.

Time reversal mirrors are not only devoted to applied physics. They can also be used in fundamental physics to solve problems in the field of wave propagation. Inverse problems can be solved by the use of a time reversal mirrors which can also be used to study multiple-scattering processes in heterogeneous media and to give some new approaches to the problem of wave localization.

Time reversal techniques may also be extended to types of waves other than acoustic waves. Some researchers in the radar community are exploring their possible application to pulsed radar, using electromagnetic waves in the microwave range. Another type of wave occurs in quantum mechanics: the quantum wavefunctions that describe all matter. Indeed, a type of retroreflection can occur when an electron wavefunction hits the boundary between a normal conductor and a superconductor. One can only speculate on what kinds of tricks would be possible if time reversal were applied to the waves of quantum mechanics.

Plenty of exploration can be done in the field of medical applications using time reversal. Abdominal and cardiac applications are limited by the motions of breathing and heartbeats which can use the time reversal technique. Also another challenge is the brain hyperthermia in which we need to focus through the skull, which severely refracts and scatters the ultrasonic beam. The porosity of the skull produces a strong dissipation – absorbing energy from the wave – and thus breaks the time-reversal symmetry of the wave equation. A new focusing technique can be developed using time reversal that adds a correction of these dissipative effects to standard time-reversal.

7. REFERENCES

- [1] T. Yu and L. Carin, "Extended-Born method for the modeling of buried voids", IEEE Trans. Geoscience and Remote Sensing, vol. 38, pp. 1320-1327, May 2000
- [2] Asch M, Kohler W, Papanicolaou G, Postel M and White B 1991 Frequency content of randomly scattered signals SIAM Review 33 pp 519-625
- [3] Asch M, Papanicolaou G, Postel M, Sheng P, and White B 1990 Frequency content of randomly scattered signals, Part I, Wave Motion 12 pp 429-450
- [4] M. Porter, P. Roux, H. Song, and W.A. Kuperman, "Tumor treatment by time-reversal acoustics," IEEE Proc. ICASSP-99, IV-2107, Phoenix, Arizona, 1999.
- [5] Bal G and Ryzhik L 2002 (preprint).
- [6] J.P. Fouque and A. Nachbin: Time-reversed refocusing of surface water waves Submitted 2002.
- [7] Blomgren P, Papanicolaou G and Zhao H 2002 Super-resolution in time-reversal acoustics JASA 111 pp 230-248
- [8] G.F. Edelmann, W.S. Hodgkiss, S. Kim, W.A. Kuperman, H.C. Song, and T. Akal, "Underwater acoustic communication using time reversal," Oceans 2001, Hawaii, 2001.
- [9] Borcea L, Tsogka C, Papanicolaou G and Berryman J 2002 Imaging and time-reversal in random media Inverse Problems 18 pp 1247-79
- [10] J.P. Fouque, J. Garnier and A. Nachbin: Time reversal for dispersive waves in random media Submitted 2003.

- [11] S. Kim, W.A. Kuperman, W.S. Hodgkiss, H.C. Song, G.F. Edelmann, T. Akal, R.P. Millane, D. Di Iorio, "A method of robust time reversal focusing in a fluctuating ocean," Oceans 2001, Hawaii, 2001.
- [12] Clouet J F and Fouque J P 1997 A time-reversal method for an acoustical pulse propagating in randomly layered media Wave Motion 25 pp 361-8
- [13] Fink M 1993 Time reversal mirrors J. Phys. D: Appl. Phys. 26 pp 1333-1350
- [14] Fink M 1999 Time-reversed acoustics Scientific American, November 1999, pp.67-93
- [15] H.C. Song, W.A. Kuperman, W.S. Hodgkiss, T. Akal, S. Kim, and G. Edelmann, "Recent results from ocean acoustic time reversal experiments," 6th European Conference on Underwater Acoustics, Gdansk, Poland, 2002.
- [16] Fouque J P and Sølna K 2002 Time-reversal aperture enhancement, submitted
- [17] Haider M A, Shipman S P and Venakides S 2002 Boundary-integral calculations of two-dimensional electromagnetic scattering in infinite photonic crystal slabs: channel defects and resonances SIAM J Appl. Math 62, pp 2129-48
- [18] Papanicolaou G, Postel M, Sheng P and White B 1990 Frequency content of randomly scattered signals, Part II, Wave Motion 12 pp 527-49
- [19] W.A. Kuperman, H.C. Song, and P. Roux, "Focal translation by frequency shift with a time-reversal mirror," First International Symposium on Physics in Signal and Image Processing (PSIP), Paris, France, 1999.
- [20] Rokhlin V 1990 Rapid solution of integral equations of scattering theory in two dimensions J Comp. Phys. 86 pp 414-439

- [21] L. Carin, R. Kapoor, C.E. Baum, "Polarimetric SAR imaging of buried landmines," IEEE Trans. Geoscience and Remote Sensing, vol. 36, pp. 1985-1988, Nov. 1998.
- [22] D. Wong and L. Carin, "Analysis and processing of ultra-wideband SAR imagery for buried landmine detection", IEEE Trans. Antennas Propagation, vol. 46, pp. 1747-1748, Nov. 1998.
- [23] L. Carin, N. Geng, M. McClure, J. Sichina, and L. Nguyen, "Ultra-wideband synthetic aperture radar for mine field detection", IEEE Antennas and Propagation Magazine (invited), vol. 41, pp. 18-33, Feb. 1999.
- [24] L. Collins, P. Yao, and L. Carin, "A Bayesian theoretic algorithm for detection of land mines", IEEE Trans. Geoscience and Remote Sensing, vol. 37, pp. 811-819, Mar. 1999.
- [25] NUMERICAL ANALYSIS (4th Edition) by Richard Burden & J. Douglas Faires.
- [26] FINITE DIFFERENCE SCHEMES & PARTIAL DIFFERENTIAL EQUATIONS by John C. Strikwerda.
- [27] http://www.gis.wau.nl/sar/sig/sar_intr.htm
- [28] <http://www.cssip.uq.edu.au/gpr2000/gpr2000tutorial.html>